Highly Conductive Multifunctional Graphene Polycarbonate Nanocomposites

Mitra Yoonessi[†,‡,*] and James R. Gaier[†]

[†]NASA Glenn Research Center, 21000 Brookpark Road, Cleveland, Ohio 44135, United States, and [‡]Ohio Aerospace Institute, 22800 Cedar Point Road, Cleveland, Ohio 44142, United States

ABSTRACT Graphene nanosheet—bisphenol A polycarbonate nanocomposites (0.027—2.2 vol %) prepared by both emulsion mixing and solution blending methods, followed by compression molding at 287 °C, exhibited dc electrical percolation threshold of ~0.14 and ~0.38 vol %, respectively. The conductivities of 2.2 vol % graphene nanocomposites were 0.512 and 0.226 S/cm for emulsion and solution mixing. The 1.1 and 2.2 vol % graphene nanocomposites exhibited frequency-independent behavior. Inherent conductivity, extremely high aspect ratio, and nanostructure directed assembly of the graphene using PC nanospheres are the main factors for excellent electrical properties of the nanocomposites. Dynamic tensile moduli of nanocomposites increased with increasing graphene in the nanocomposite. The glass transition temperatures were decreased with increasing graphene for the emulsion series. High-resolution electron microscopy (HR-TEM) and small-angle neutron scattering (SANS) showed isolated graphene with no connectivity path for insulating nanocomposites and connected nanoparticles for the conductive nanocomposites. A stacked disk model was used to obtain the average particle radius, average number of graphene layers per stack, and stack spacing by simulation of the experimental SANS data. Morphology studies indicated the presence of well-dispersed graphene and small graphene stacking with infusion of polycarbonate within the stacks.

KEYWORDS: nanocomposite · electrical conductivity · graphene · scattering

Polymer nanocomposite applications require enhancement of the thermal, mechanical, and electrical properties. Electrical properties of nanocomposites are crucial in many aerospace applications including lightning strike dissipation in air vehicles and electrical charge mitigations in space vehicles in the charged space environment. In addition, robust mechanical properties are necessary in a wide range of temperatures for fundamental structural material components.

Polycarbonate is an engineering thermoplastic with outstanding mechanical properties, high stiffness and high modulus, as well as excellent thermal properties and good dimensional stability.[1,2] Its mechanical properties and impact strength combined with high optical clarity make it an excellent candidate for a wide range of applications including air vehicle components.[1,2]

High aspect ratio, conductive nanoparticles such as single-wall carbon nanotubes and multiwall nanotubes have been incorporated in bisphenol A polycarbonate (BPA-PC) to improve its electrical and mechanical performance.[3−8] Electrical conductivity and percolation threshold in a polymer nanocomposite is related to the inherent conductivity of the nanoparticle, concentration, aspect ratio, extent of aggregation and dispersion, orientation, and directed assembly of the nanoparticles in the polymer matrix. The extent of nanoparticle dispersion and aggregation has a significant impact on the final properties of the nanocomposites and is directed by the dispersion method. Addition of highly conductive and high modulus nanoparticles often results in increasing the composite's modulus and stiffness.

Graphene is a two-dimensional monatomic thin sheet with a large lateral dimension sp^2-hybridized carbon nanostructure.[9−17] Natural graphite is made of stacked graphene nanosheets with extremely large lateral dimensions. Each graphene layer consists of covalently bonded six-membered sp^2-hybridized carbon rings stacked by van der Waals forces in 3.4 Å spacing. Graphene's quasi-two-dimensional monatomic planar structure provides unique transport and opto-electronic properties.[9−17] This includes a thermal conductivity of ~3000 W/mK,[12,13] in-plane stiffness of 1060 GPa,[12,13] resistivity in the range of 50 $\mu\Omega \cdot$ cm, a theoretical surface area of 2630 m^2/g, 98.7% transmission normal to the incident beam for the first layer, and 2.3% reduction for the consecutive layers in vacuum. Graphene's charge carrier mobility is ~20 000 cm^2/s, and

*Address correspondence to mitra.yoonessi@nasa.gov.

Received for review August 9, 2010 and accepted November 02, 2010.

Published online November 17, 2010.
10.1021/nn1019626

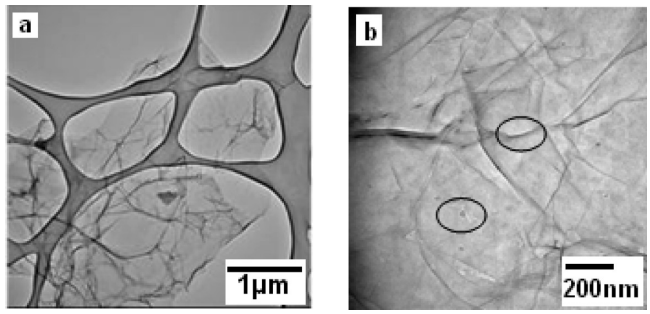

Figure 1. HR-TEM micrograph of graphene nanosheets. (a) Graphene nanosheets with micrometer-sized lateral dimensions (~9.2 × 15.1 μm). (b) Exfoliated graphene nanosheet. Circles are showing defects, roughness and wrinkling.

concentrations up to 10^{13} cm^{-2} are weakly temperature-dependent.[12,13]

Chemically modified graphene polystyrene nanocomposites have been prepared *via* reduction of phenyl isocyanate-treated graphene oxide in the presence of the polystyrene exhibit percolation of 0.1 vol % and conductivity of 0.001 S/cm at 1 vol %.[12] The percolation threshold of graphite nanosheet/poly(methyl methacrylate) films prepared by *in situ* polymerization was reported as 0.31 vol %.[18] The electrical conductivity of the epoxy-functionalized graphene/epoxy nanocomposites exhibited a 5 order increase with 0.5 wt % epoxy-functionalized graphene.[19] Grafting polystyrene to graphene oxide *via* atom transfer radical polymerization (ATRP) yielded composites with 9−18 °C increases in T_g due to the confinement effects of polystyrene (PS) chains.[20] Graphene oxide polyvinyl alcohol nanocomposites, prepared in water solution method, exhibited 76% increase in tensile strength and 62% improvement in modulus with 0.7 wt % of graphene oxide in the composite.[21] Polycarbonate thermally expanded graphene oxide nanocomposites prepared by melt compounding showed a surface resistivity percolation at 1.25 wt % and surface resistivity values of 8×10^5 and 2×10^5 Ω for 2 and 3 wt % for disk nanocomposites.[22]

Correlation between the electrical conductivity of graphene bisphenol A polycarbonate nanocomposites and their morphology is the objective of this study as a model system. This study also compares the effects of nanostructure directed assembly of graphene nanosheets *via* an emulsion mixing method with the solution blending method for PC nanocomposite preparation. The aspect ratio, nanostructure and morphology, inherent conductivity, extent of dispersion, and aggregation of the conductive component ultimately define the percolation volume fraction of the nanocomposites. This approach explores the effects of morphology design of the conductive component within the insulating polycarbonate matrix. Graphene/PC nanocomposites prepared by emulsion mixing and solution blending are called E-G-PC nanocomposites and S-G-PC nanocomposites, respectively.

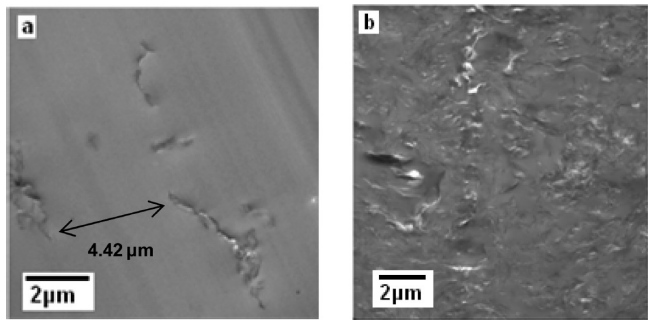

Figure 2. HR-TEM of the (a) 0.27 and (b) 2.2 vol % S-G-PC nanocomposites.

RESULTS AND DISCUSSION

Graphene. Rapid thermal expansion of graphite oxide by Aksay *et al.* resulted in well-separated graphene nanosheets.[15−17] The HR-TEM micrographs of the reduced graphene nanosheets show a lateral dimension of 9.2 × 15.1 μm with folding and wrinkling (Figure 1a,b). The folding and wrinkling is due to the defects resulting from the preparation method.[15−17] Graphene nanosheets have lateral dimensions between 700 nm and 15 μm with an average size of ~3 μm based on HR-TEM studies. The preparation method of graphene under high pressure and high temperature results in overcoming van der Waals forces between the large stacks and separation of the nanolayers into individual or small stacks of graphene with highly oxygenated functional groups.[15−17] This processing method results in defects and rearrangements of hexagonal carbon rings into carbon rings with 5 or 7 carbon atoms which cause wrinkling and higher roughness of the graphene.[15] The reduced graphene used in this study had 7% atomic oxygen based on high-resolution spectra of the XPS (Supporting Information). Peak deconvolution of the C1s binding energies resulted in similar findings by Aksay's group,[15−17] indicating a variety of C−O and C═O functional groups.

POLYMER NANOCOMPOSITE CHARACTERIZATION

TEM. ***S-G-PC Nanocomposites.*** The morphology of the S-G-PC nanocomposites is a random dispersion of highly delaminated conductive graphene nanosheets demonstrated by HR-TEM in Figure 2a,b for 0.27 and 2.2 vol % S-G-PC nanocomposite, respectively. Figure 2a shows isolated graphene nanosheets and a few small polycarbonate-infused graphene nanosheet stacks within the polycarbonate matrix. This morphology results in electrical insulation behavior. Random dispersion of large particle number densities of graphene and graphene stacks in 2.2 vol % S-G-PC nanocomposites is demonstrated in Figure 2b. This morphology generates a random electrical transport path within the insulating PC matrix.

E-G-PC Nanocomposites. Conductive graphene nanoparticles are positioned on the polycarbonate microsphere

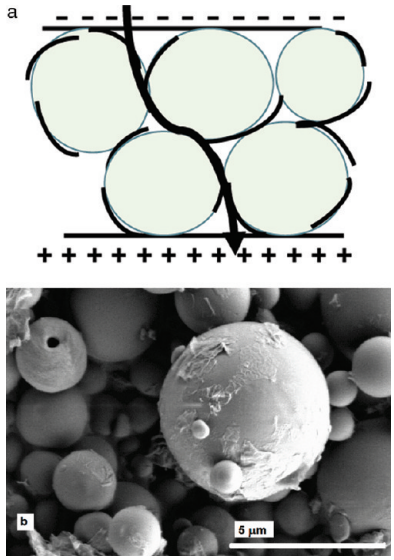

Figure 3. (a) Schematic of the directed assembly of graphene nanosheets on the polymer microspheres to generate an electron transport path. (b) SEM micrograph of graphene nanosheets on the PC microspheres.

surfaces in the E-G-PC nanocomposites by this preparation method (Figure 3a). Positioning multiwall carbon nanotubes on the surface of the PC emulsions has been studied.[4] This morphology provides a conductive path for the electron transport and generates an excluded volume of insulating polymer. Figure 3b exhibits the positioning of graphene nanosheets on the PC microspheres by scanning electron microscopy. This design of morphology for graphene polycarbonate nanocomposites leads to much lower percolation volume fraction (~0.14 vol %) compared to solution blending (0.38%).

Figure 4a shows the 0.27 vol % and Figure 4b and c show the 2.2 vol % E-G-PC nanocomposite. Curved and bent graphene nanolayers and graphene layer stacks are present in close proximity (Figure 4b,c). The location of the graphene nanolayers and stacks in the polycarbonate shows the directed assembly of the graphene that is achieved through emulsion mixing. The graphene nanolayers and stacks are generating a pathway for charge carrier transport.

Electrical Conductivity. The ac and dc conductivity measurements were performed for all nanocomposites. The resistivity values were calculated as the slope of $I-V$ curve and which were linear for all S-G-PC nanocomposites and almost linear for E-G-PC. Figure 5 exhibits the

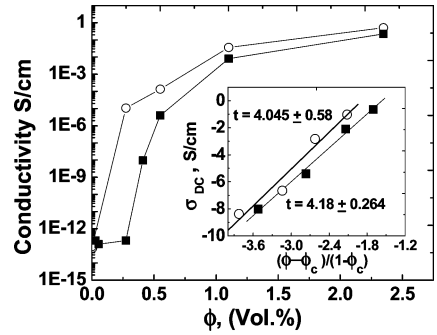

Figure 5. Direct current conductivity percolation data of graphene PC nanocomposite prepared by (a) emulsion mixing (○) and (b) solution mixing (■).

dc conductivity as a function of graphene volume fraction at room temperature and demonstrates the percolation behavior for both types of mixing. Percolation is defined where the conductivity suddenly increases at a critical graphene concentration (ϕ_c) where the conductive nanoparticles are in close enough proximity to generate a pathway for charge carrier transport. The percolation threshold depends on the concentration of the conductive nanoparticle, the extent of nanoparticle dispersion and/or aggregation, nanoparticles aspect ratio, their orientation, and directed self-assembly. The percolation volume fraction has been also reported as the theoretically calculated transition point of the percolation curve.[18,33,26] This results in ~0.14 and ~0.38 vol % for E-G-PC and S-G-PC nanocomposites, respectively. The conductivity values of 0.14 and 0.27 vol % E-G-PC nanocomposites increased to 1.028×10^{-9} and 3.96×10^{-6} S/cm from 2.05×10^{-13} S/cm for neat PC when the extent of aggregation and the spatial arrangements of the graphene nanoparticles were directed using emulsion method. This is the lowest percolation reported for PC/graphene nanocomposites[22] and almost the lowest for graphene nanocomposites. Only the reported value for graphene in the graphene polystyrene nanocomposite from Ruoff *et al.* is lower.[12]

Percolation bond theory suggests the following form relating the conductivity to the volume fraction of the nanoparticles:[23−25]

$$\sigma_{DC} = \sigma_f[(\phi - \phi_c)/(1 - \phi_c)]^t$$

where ϕ_c is the percolation volume fraction, σ_f is the conductivity of the nanoparticle additive, and t is the critical exponent.[23−25] This equation is valid for the $\phi >$

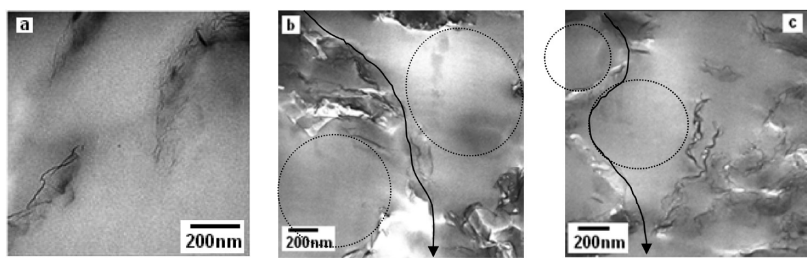

Figure 4. HR-TEM of the 0.27 (a) and 2.2 vol % (b,c) E-G-PC nanocomposites.

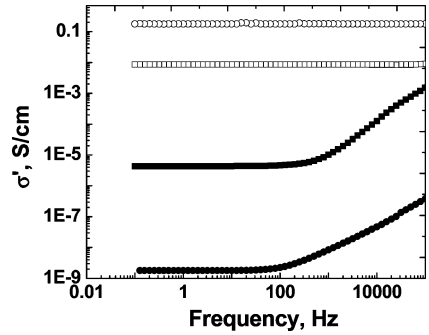

Figure 6. Frequency-dependent conductivities for S-G-PC nanocomposites with graphene volume fractions of 0.41 (●), 0.55 (■), 1.1 (□), and 2.35 (○).

ϕ_c and when $\phi - \phi_c$ is small. A linear fit to the logarithmic plot of conductivity *versus* $(\phi - \phi_c)/(1 - \phi_c)$ results in $t = 4.18 \pm 0.26$ and a nanoparticle conductivity, σ_f, of $10^{6.55\pm0.69}$ S/cm for the S-G-PC nanocomposites. Values of $t = 4.04 \pm 0.58$ and σ_f of $10^{6.39\pm1.32}$ S/cm result for the E-G-PC nanocomposite series. In comparison, the percolation bond model resulted in $t = 2.74 \pm 0.2$ for the chemically modified graphene PS nanocomposites and nanoparticle conductivity of $10^{2.92\pm0.52}$ S/cm.[12] Thus, this simulation results in 3−4 orders of magnitude higher values of graphene nanoparticle inherent conductivity compared to the earlier report.[12] The percolation bond model resulted in $t = 3.47 \pm 0.64$ for graphene nanosheet PMMA nanocomposites.[18] The high t value is attributed to extreme geometries of conducting nanoparticle[23] and could be an indication of a different electron transport behavior. Higher values of critical exponent of 4.1 and 4.5 have been reported for pulsed laser vaporization SWNT (PLV) and oxidized PLV poly[(*m*-phenylenevinylene)-*co*-[(2,5-dioctyloxy-*p*-phenylene)vinylene]] (PmPV) nanocomposites.[26] The t values of 1.36 for PmPV and polyvinyl alcohol (PVA) carbon nanotube,[28] 1.33 and 1.42 for separate PMM-polyaniline network,[29,30] and 2 and 2.9 for HiPco and oxidized HiPco-PmPV[26] have been reported. Values of $t = 3.1$ and 3.2 for surface-modified carbon nanofiber polyimide nanocomposites have also been reported.[31]

AC Conductivity. ***S-G-PC Nanocomposites.*** S-G-PC nanocomposites with high resistivity were beyond the instrument measurement capability. Figure 6 shows the real component of conductivity for the S-G-PC nanocomposite series as a function of frequency. The nanocomposite with 0.41 vol % graphene is above the percolation volume fraction. Graphene nanocomposites containing 0.55 vol % graphene exhibit a frequency-independent behavior followed by a frequency-dependent behavior (dielectric) at critical frequency, ω_c. The critical frequency is defined as $\sigma_{\omega_c} = 1.1\ \sigma_{DC}$ by Kilbride *et al.*[28] S-G-PC nanocomposites with 1.1 and 2.2 vol % graphene exhibited a frequency-independent behavior. The plateau values of the frequency-independent conductivity, $\sigma_{ac,0}$, are attributed to the dc conductivity, σ_{DC}, and have been compared in Table 1. There is good agreement between the ac and dc conductivity measurements for all nanocomposites. The maximum conductivity achieved by the solution blending method with 2.2 vol % graphene was 0.226 S/cm in the conductive plateau regime, which is unprecedented in the literature for graphene nanocomposites. It should be noted that these conductivity values have been measured for bulk graphene nanocomposites where three-dimensional dispersion of graphene exists (sample thickness ~1 mm) and not composite thin films.

TABLE 1. Summary of AC and DC Conductivity, σ, Values Comparison as a Function of Volume Fraction (AC Conductivity Exponent Values (*s*) Are Also Reported as a Function of Volume Fraction)

vol %	wt %	σ_{DC}, S/cm	$\sigma_{ac,0}$, S/cm	*s*
S-G-PC nanocomposites				
0.41	0.75	9.45×10^{-9}	1.79×10^{-9}	0.78
0.55	1	3.96×10^{-6}	4.37×10^{-6}	0.76
1.1	2	0.00794	0.0086	
2.2	4	0.226	0.179	
E-G-PC nanocomposites				
0.27	0.5	1.07×10^{-5}	5.26×10^{-5}	0.92
0.55	1	1.34×10^{-4}	9.58×10^{-5}	0.57
1.1	2	0.0363	0.0159	
2.2	4	0.512	0.557	

Figure 7 shows the real component of ac conductivity for the 0.55 vol % S-G-PC nanocomposite as a function of temperature and normalized with respect to $\sigma_{ac,0}$ and critical frequency ω_c using extended pair approximation model defined by the following equation.[28,25,32]

$$\sigma(\omega)/\sigma_{DC0} = 1 + k(\omega/\omega_c)^s \quad 0 < s < 1$$

Here, k is the arbitrary parameter and s is the exponent value.[25,28,32] A different form of this model has also been utilized as the ac universality law.[26,27,31−34] This fitting resulted in a master curve for the S-G-PC nanocomposites. The s values are listed in Table 1 and compared for the nanocomposites. The conductivity decreased with increasing temperature, which was more significant when the temperature increased to 145 °C. The

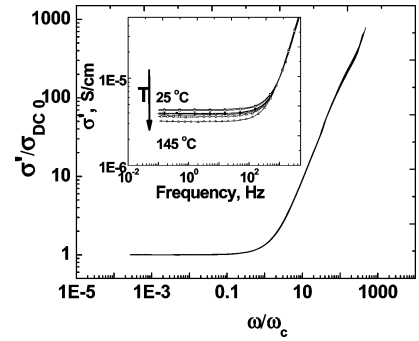

Figure 7. Frequency-dependent behavior of the 0.55 vol % S-G-PC nanocomposite as a function of temperature from 25 to 145 °C. The data are normalized with respect to σ_{DC} and critical frequency, ω_c.

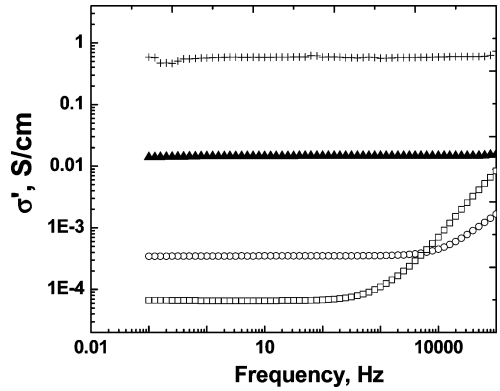

Figure 8. Real component of the conductivity, σ′, *vs* frequency for the E-G-PC nanocomposites with graphene volume fractions of 0.27 (□), 0.55 (○), 1.1 (▲), and 2.2 (+).

more significant change occurs at 145 °C, which is close to polymer's glass transition temperature (~165 °C). Meanwhile, the effects of conductivity changes for the nanocomposites in the conductive range, 1.1 and 2.2 vol % graphene nanocomposites were insignificant.

The decrease in the conductivity can be attributed to the thermal effects on the physical properties of the polymer, thermal effects on the electron transport mechanisms, and temperature effects on the filler−filler junction resistance. The more significant change of the conductivity at the percolation regime suggests that the polymer effects are the dominant effects in the change of conductivity. The decrease in the conductivity is attributed to the thermal expansion of the polymer, in addition to the onset of vibrational motion of methyl groups at lower temperatures, and long-range chain segmental motion. The onset of short-range chain segmental motion and an increase in the free volume starts when the temperature increased close to the glass transition temperature. This phenomena led to a more significant decrease in conductivity.

E-G-PC Nanocomposites. Figure 8 shows the real conductivity component for the E-G-PC nanocomposite series as a function of frequency at room temperature. The 0.27 vol % graphene PC nanocomposite is above percolation. The 0.27 and 0.55 vol % E-G-PC nanocomposites exhibit a frequency-independent behavior followed by the frequency-dependent behavior occurring at the critical frequency. The E-G-PC nanocomposites with 1.1 and 2.2 vol % graphene exhibited frequency-independent behavior with conductivity values up to 0.0363 and 0.512 S/cm, respectively. These values are the highest reported in the literature for only 1.1 and 2.2 vol % of graphene in the polymer matrix. Figure 9 shows the conductivity normalized data for 0.27 vol % E-G-PC nanocomposite from 25 to 145 °C. Table 1 shows the comparison between $\sigma_{ac,0}$ obtained from ac measurements compared with direct dc measurements.

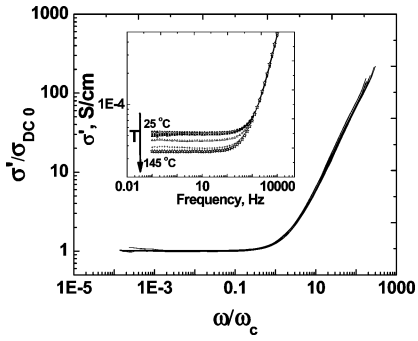

Figure 9. Frequency-dependent behavior of 0.27 vol % E-G-PC nanocomposite as a function of temperature from 25 to 145 °C. The data are normalized with respect to σ_{DC} and critical frequency, ω_c, where σ' is the real component of conductivity and $\sigma_{DC,0}$ is the frequency-independent conductivity at low frequency regime.

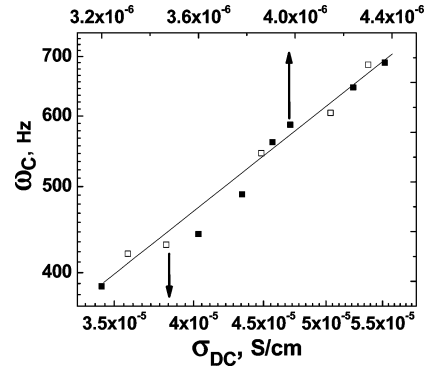

Figure 10. Plot of critical frequency *vs* σ_{DC} for the 0.55 vol % S-G-PC nanocomposite (□) and the 0.27 vol % E-G-PC nanocomposite (■).

The higher frequency associated with local charge transport phenomena is a function of frequency obeying a power law behavior with exponent of *s*. Comparing the room temperature ac conductivity data with this model results in *s* exponent values of 0.78 and 0.76 for the 0.41 and 0.55 vol % S-G-PC nanocomposites. Their conductivities were on the order of 10^{-9} and 10^{-6} S/cm, respectively (Table 1). The 0.27 vol % E-G-PC nanocomposites exhibit an *s* value of 0.92. The *s* value was lower, 0.57, when the graphene content of the nanocomposite increased to 0.55 vol % and the nanocomposite's conductivity was on the order of 10^{-4} S/cm. The values of *s* close to 1 have been reported for insulating

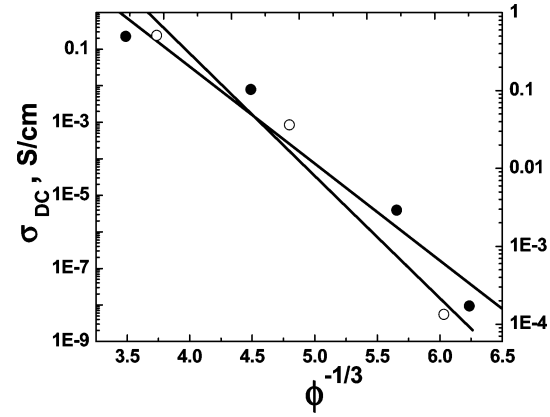

Figure 11. Plot of the log of the electrical conductivity vs concentration, $(\phi)^{-1/3}$, E-G-PC nanocomposite (○), and S-G-PC nanocomposite (●).

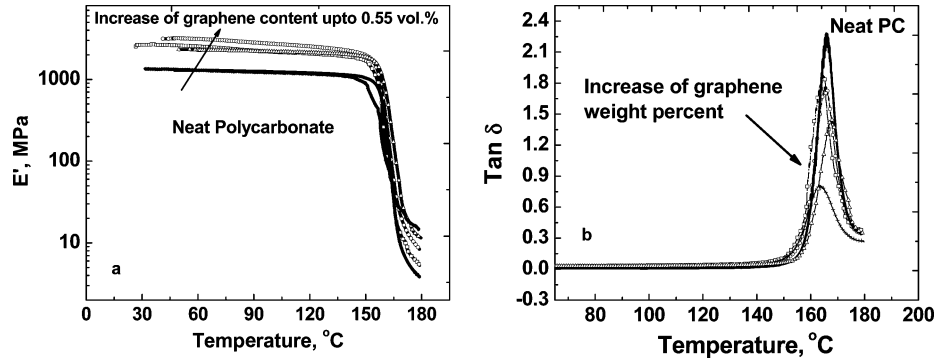

Figure 12. Dynamic properties of S-G-PC nanocomposites. (a) Tensile storage moduli. (b) Damping tan delta (neat PC (−), 0.27 vol % (□), 0.55 vol % (○), 1.1 vol % (Δ), and 2.2 vol % (+) nanocomposites).

polymers. The *s* value was reported to decrease with increasing conductive nanoparticle loading in high-density polyethylene.[33] We also observed the same decreasing *s* value with increasing graphene content and increasing nanocomposite conductivity for S-G-PC nanocomposites. However, the E-G-PC nanocomposite has a high *s* value for the 0.27 vol % composite. Values of *s* in the range of ~0.72 have been proposed for three-dimensional nanostructure with polarization effects between nanoparticles and value of $s \sim 0.58$ where anomalous diffusion between clusters exists.[33] The frequency-dependent conductivity is considered in the percolating regime where a physical network of the graphene starts to form. There is a finite correlation length that charge carriers can travel. The values of *s* exponents ranged from 0.57 to 0.78, in agreement with the expected range given by percolation theory (0.58−0.7).[23,33] Only the E-G-PC nanocomposite exhibits a higher *s* value of 0.92. Higher *s* values also have been attributed to the hopping mechanism.[34] As the concentration of the graphene is increased to 1.1 and 2.2 vol %, the connected electron transport path forms *via* a network of graphene nanosheets where the electrical characteristics are no longer a function of frequency.

The critical frequency is approximated by a power law equation, $\omega_c \sim \sigma_{DC}{}^b$, where *b* is a constant with values close to 1.[27,33] A linear dependence of log ω_c *versus* log σ_{DC} with exponent values of ~0.99 ± 0.1 and 1.01 ± 0.1 was obtained for 0.55 vol % S-G-PC and 0.27 vol % E-G-PC nanocomposites (Figure 10). This is in agreement with the theory and similar to the value reported for epoxy/CNT nanocomposites (~0.99).[32] This has been reported for disordered solids.[35,36]

According to theoretical considerations, there is a linear relation between σ_{DC} and $\phi^{-1/3}$ in logarithmic scale when the conductivity is limited by a tunneling barrier ($\log(\sigma_{DC} \sim \phi^{-1/3})$. The charge carrier can travel through the barrier insulating polymer gap, a distance longer than the nanoparticle length. This strongly agreed with the linear behavior obtained from the logarithmic plot of conductivity *versus* $\phi^{-1/3}$ for both series of nanocomposites (Figure 11).

Dynamic Mechanical Properties. ***S-G-PC Nanocomposites.*** The tensile storage moduli below the glass transition temperature increased with increasing nanocomposite graphene content up to 0.55 vol % graphene (Figure 12a). These moduli start to decrease when the graphene content increased to 1.1 vol % and further decreased to the range of neat PC modulus when the graphene content increased to 2.2 vol %. This can be attributed to the large particle number density of graphene, poor surface wetting of the graphene sheets with the polymer molecules, and presence of agglomerates. At higher graphene concentrations, the high particle number density of the graphene nanosheets results in reducing the cohesiveness of the material and, therefore, lowers the stiffness. The moduli of the S-G PC

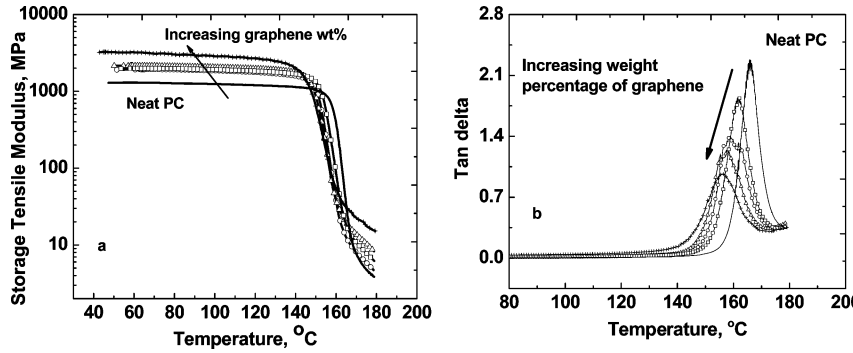

Figure 13. Dynamic properties of E-G-PC nanocomposites. (a) Tensile storage moduli. (b) Damping tan delta (neat PC (−), 0.27 vol % (□), 0.55 vol % (○), 1.1 vol % (Δ), and 2.2 vol % (+) nanocomposites).

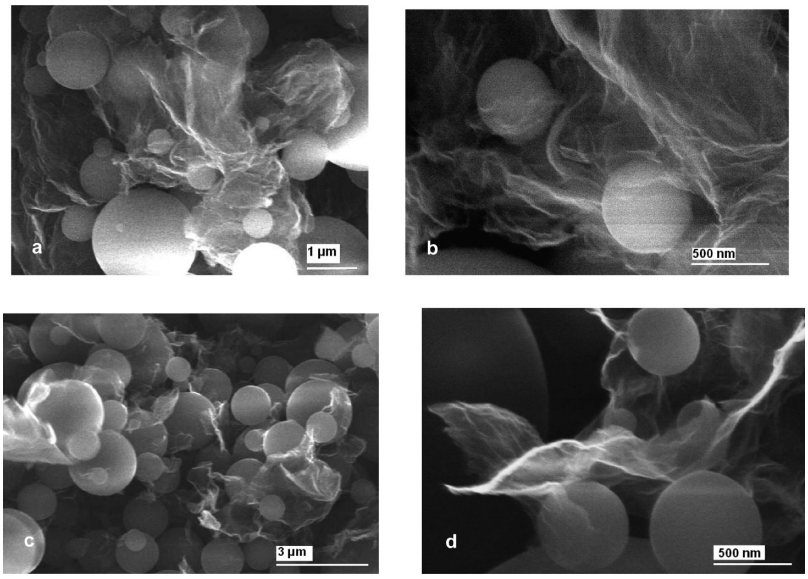

Figure 14. SEM of the 0.55 vol % (a,b) and 1.1 vol % E-G-PC microspheres covered with graphene.

nanocomposites above T_g increased with increasing graphene content similar to E-G-PC nanocomposites.

The glass transition values of the neat PC and the nanocomposites with 0.27, 0.55, 1.1, and 2.2 vol % were 165.8 165, 166.2, 168, and 163.7, respectively (Figure 12b). Increasing graphene content resulted in slight increase in the T_g for 0.55 and 1.1 vol % S-G-PC nanocomposites and then a decrease in the T_g for 2.2 vol % S-G-PC nanocomposite. The nanocomposite containing 2.2 vol % graphene had lower T_g compared to the neat PC. Addition of graphene resulted in a decrease in the area under the damping peak similar to the E-G-PC nanocomposites. A decrease in the area under damping has been previously reported for PC/multiwall nanocomposites.[8]

E-G-PC Nanocomposites. The tensile storage moduli of the E-G-PC nanocomposites increased with increasing graphene content up to 2.2 vol %, illustrating the graphene reinforcing effects (Figure 13a). The increase in modulus was more significant for the 2.2 vol % graphene PC nanocomposite. The modulus above T_g increased with increasing graphene content due to filler reinforcing effects.

Figure 13b shows the damping tan delta of the E-G-PC graphene nanocomposites as a function of temperature. The T_g values of the nanocomposites decreased with increasing graphene content. The T_g values of PC, 0.27, 0.55, 1.1, and 2.2 vol % E-G-PC nanocomposite, were 165.8, 161.8, 158.8, 156.64, and 156.1 °C, respectively. This could be due to poor wetting of the graphene surface with the polycarbonate molecules or the presence of surfactant residue on the graphene surface acting as plasticizer. The area under the tan delta curve is also decreased with increasing graphene content. Increasing graphene content will increase the rigidity and reduce the damping characteristics.

MORPHOLOGY

Nanostructure of Nanocomposites. ***SEM.*** Figure 14 shows the 0.55 vol % (panels a and b) and the 1.1 vol % (panels c and d) graphene/PC microspheres. The polycarbonate microspheres' diameters were in the range of 0.5−5 μm with high polydispersity. Conductive graphene nanosheets, in the form of single or a few nanosheets, are wrapped around a PC microsphere, where ultimately the conductive path for electron transport is generated. The graphene nanosheets show wrinkling and irregular lateral shape.

SANS. The extent of aggregation or dispersion, average dimensions, and the thickness of graphene in S-G-PC nanocomposites was examined using USANS and SANS in the q range of $3.96 \times 10^{-5} < q$ (1/Å) < 0.1. The contrast between polycarbonate (repeat unit: $C_{16}O_3H_{14}$, $d = 1.2$ g/mL) with a scattering length density, ρ_{PC}, of 2.03×10^{-6} Å^{-2} and graphene (C, $d = 2.2$ g/mL) with a ρ_c value of 7.33×10^{-6} Å^{-2} is $\Delta\rho = 5.3 \times 10^{-6}$ Å^{-2}. This results in scattering spectra from a two-

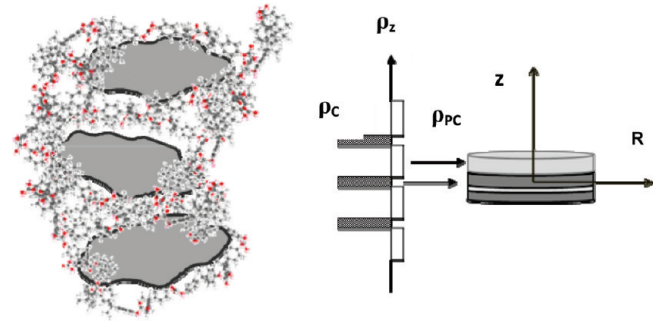

Figure 15. Graphene nanosheets are considered as thin disks with large lateral dimension embedded in the polycarbonate matrix.

TABLE 2. Summary of the Simulation Results of the SANS Experimental Data with a Stacked Disk Model

materials S-G-PC nanocomposites, vol %	average radius, *R*, μm	number of layers per stack, *N*	graphene stack spacing, nm
0.1	2.65	7	25.7
1.1	1.68	12	18.7
2.2	1.75	14	16.9

phase structure (Figure 15).[37−39] The irregular large lateral dimension and small thickness of graphene nanosheets were assumed to be a thin disk.[38] Therefore, a previously developed stacked disk model[40] utilized for Montmorillonite clay[40,41] is employed here to quantify the size, aggregation, and dispersion of the graphene within the polycarbonate matrix. In this model, it is assumed that the graphene nanosheets are present in the form of finite stacks with infusion of polycarbonate between the layers, resulting in expansion of the graphene nanosheets layers. These stacks are dispersed through the polymer matrix.

Figure 16 shows the scattering profile for the 0.1, 1.1, and 2.2 vol % S-G-PC nanocomposites. The 0.1 vol % nanocomposite exhibited a Guinier plateau in the low q range, indicating that noninteracting particles exist. The Guinier approximation,[37−39] $\ln I = \ln I_0 - q^2R_g^2/3$, can be used to estimate the particle radius of gyration, R_g, where I is the scattering intensity and I_0 is the extrapolated scattering intensity.[37−39] This linear fit results in average R_g of 1.47 ± 0.43 μm. The average particle radius, R, can be deduced from the approximation $\langle R_g\rangle^2 = 1/2(R)^2$ assuming a thin disk geometry. This leads to particle radius of 2.08 μm. The stacked disk model was utilized to estimate the average radius of the graphene nanosheets, number of layers per stack of graphene, and layer separation. The equations and the theory for this model have been established earlier[40] and are presented in the Supporting Information for clarity of the discussion. The results of this modeling are listed in Table 2. The increased scattering at lower q values is due to aggregates or larger graphene nanosheets in the nanocomposite. The Gaussian standard deviation was assumed to be 0.95 for all simulations due to the high polydispersity of the graphene geometrical characteristics. The radius predicted by the stacked disk model was 2.65 μm for 0.1 vol % S-G-PC nanocomposite, which was in agreement with the radius obtained from the Guinier approximation of 2.08 μm. The graphene stack spacing decreased from 25.7 to 18.7 nm and further decreased to 16.9 nm with increasing graphene concentration in the nanocomposite. The average number of graphene layers in the graphene stack increased from 7 for 0.1 vol % to 12 for 1.1 vol % and 14 for 2.2 vol % S-G-PC nanocomposites with increas-

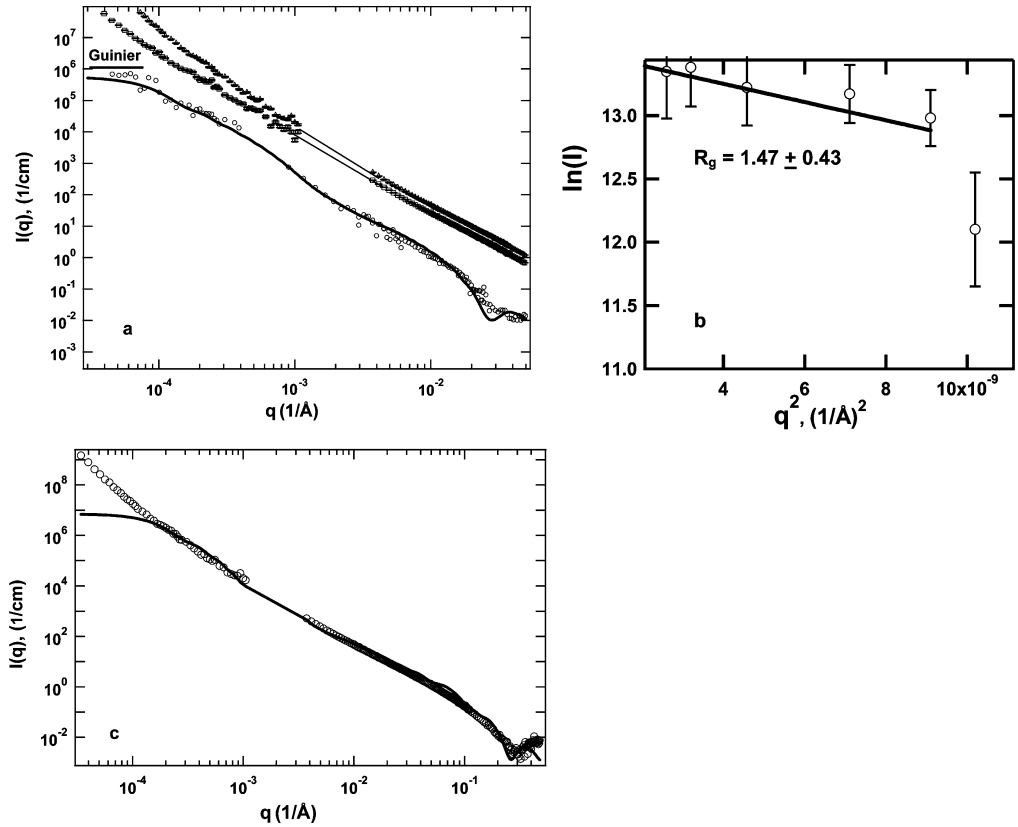

Figure 16. (a) Scattering intensity *vs* wave vector, *q*, of the S-G-PC nanocomposites, 0.2 (○), 1.1 vol % (Δ), 2.2 vol % (□). The theoretical representation of stacked disk model (−) is compared to the 0.1 vol % graphene nanocomposites. (b) Guinier plot of ln *I vs* q^2 for $q < 9.54 \times 10^{-5}$ 1/Å for the 0.1 vol % S-G-PC nanocomposite. (c) Comparison of the theoretical representation of stacked disk model with the experimental data of 2.2 vol % S-G-PC nanocomposite.

ing graphene concentration. The model prediction for the average radius of the 0.1 vol % nanocomposite was 2.65 μm, while the average radii predicted for 1.1 and 2.2 vol % nanocomposites were 1.68 and 1.75 μm.

CONCLUSIONS

Graphene nanocomposites with low percolation limit values of ~0.14 and ~0.38 vol % from emulsion mixing and solution blending, respectively, were prepared. Graphene nanocomposites with 1.1 and 2.2 vol % graphene were in the conductive regime with exceptionally high conductivities. The ac conductivity measurements exhibited good agreement with the dc conductivities. The linearity of the conductivity *versus* the concentration, $\phi^{-1/3}$, indicates that charge carrier tunneling occurring along the correlating distance between the nanoparticles exists. The nanocomposites exhibited improvement in tensile moduli. Simulation of the SANS data with the stacked disk model indicated that the average radius of the graphene particles ranged from 1.7 to 2.7 mm, and as the concentration increased from 0.1 to 2.2 vol %, the number of graphene sheets in a stack increased from 7 to 14, where the spacing within a stack decreased from 27 to 17 nm. HR-TEM provided information about the dispersion and extent of dispersion of graphene within the polycarbonate graphene nanocomposites.

METHODS

Materials. BPA-PC, Lexan 121 (M_w = 26 301 g/mol, PDI = 1.72) and conductive graphene platelets[15−17] (VO-100), and BET surface area of 700−1300 m^2/g, were generously donated by Sabic Innovative Plastics and Vorbeck Inc. Triton X-100, chloroform, methylene chloride, polyvinyl pyrrolidone (PVP, M_w 360 000 g/mol) were provided from Sigma and used without any modification.

Nanocomposite Preparation Methods. Solution blending: Dilute graphene chloroform dispersions (1×10^{-4} g/mL) were sonicated for 1.5 h followed by 30 min sonication of the mixture of this dispersion and polycarbonate chloroform solutions (0.1 g/mL). The PC graphene formed powders (0.027−2.2 vol % of graphene) after chloroform removal. The powder was formed into 1 in. diameter ~1 mm thick circular disks by compression molding at 287 °C and 32 psi for 30 min. These nanocomposites are called S-G-PC nanocomposites.

Emulsion mixing: Polycarbonate microemulsions were formed according to the previously published procedure[4] by mixing polycarbonate solution (2 g/40 mL methylene chloride) with a solution of 5 g of PVP in 200 mL of DI water (8 MΩ) under extreme agitation (homogenizer and stirring) and mild heat. Graphene was added to a Triton X-100 aqueous solution and sonicated for 15 min. Then, this dispersion was added to the stabilized PC microemulsion and stirred. The dispersion was filtered, washed several times, and dried. Microsphere composite powders of 0.027−2.2 vol % were compression molded with the same protocol as S-G-PC nanocomposites and called E-G-PC nanocomposites.

Acknowledgment. The NASA Aeronautics-Subsonic Fixed Wing Program is thanked for the funding through Contract NNC07BA13B. M.A. Meador is thanked for the invaluable support. R. Rogers, D. Hull, F. Sola, and D. Scheiman of NASA-GRC, Y. Lin and D. Mildner of NCNR-NIST are thanked. R. Ruoff and J. Potts of University of Texas—Austin and S. Kline of NCNR-NIST are thanked for their helpful comments. NIST is thanked for funding (Proposal S23-59) to conduct neutron scattering experiments which were supported by National Science Foundation under agreement DMR-9986442. The mention of commercial products does not imply endorsement by NIST nor does it imply that the materials or equipment identified are necessarily the best available for the purpose.

Supporting Information Available: Characterization methods, SANS background and stacked disk model equations, XPS data of the graphene, and WAXS data of graphene and nanocomposites. This material is available free of charge *via* the Internet at http://pubs.acs.org.

REFERENCES AND NOTES

1. Hudgin, D. E.; Bendler, T. *Handbook of Polycarbonate Science and Technology*; Marcel Dekker Inc.: New York, 2000.
2. Alegria, A.; Mitxelena, O.; Colmenero, J. On the Molecular Motions Originating from the Dielectric γ-Relaxation of Bisphenol-A Polycarbonate. *Macromolecules* **2006**, *39*, 2691–2699.
3. Alig, I.; Skipa, T.; Lellinger, D.; Potschke, P. Destruction and Formation of a Carbon Nanotube Network in Polymer Melts: Rheology and Conductivity Spectroscopy. *Polymer* **2008**, *49*, 3524–3532.
4. Jung, R.; Park, W. I.; Kwon, S.-M.; Kim, H.-S.; Jin, H.-J. Location-Selective Incorporation of Multiwalled Carbon Nanotubes in Polycarbonate Microspheres. *Polymer* **2008**, *49*, 2071–2076.
5. Kim, K. H.; Woon, H. J. A Strategy for Enhancement of Mechanical and Electrical Properties of Polycarbonate/Multi-walled Carbon Nanotube Composites. *Carbon* **2009**, *47*, 1126–1134.
6. Skipa, T.; Lellinger, D.; Böhma, W.; Saphiannikova, M.; Alig, I. Influence of Shear Deformation on Carbon Nanotube Networks in Polycarbonate Melts: Interplay between Build-up and Destruction of Agglomerates. *Polymer* **2010**, *51*, 201–210.
7. Wu, T.-M.; Chen, E.- C.; Lin, Y.-W.; Chiang, M.-F.; Chang, G.-Y. Preparation and Characterization of Melt-Processed Polycarbonate/Multiwalled Carbon Nanotube Composites. *Polym. Eng. Sci.* **2008**, *48*, 1369–1375.
8. Sung, Y. T.; Kum, C. K.; Lee, H. S.; Byon, N. S.; Yoon, H. G.; Kim, W. N. Dynamic Mechanical and Morphological Properties of Polycarbonate/Multi-walled Carbon Nanotube Composites. *Polymer* **2005**, *46*, 5656–5661.
9. Li, X.; Wang, X.; Zhang, L.; Lee, S.; Dai, H. Chemically Derived, Ultrasmooth Graphene Nanoribbon Semiconductors. *Science* **2008**, *319*, 1229–1232.
10. Geim, A. K. Graphene: Status and Prospects. *Science* **2009**, *324*, 1530–1534.
11. Castro Neto, A. H.; Guinea, F.; Peres, N. M. R.; Novoselov, K. S.; Geim, A. K. The Electronic Properties of Graphene. *Rev. Mod. Phys.* **2009**, *81*, 109–162.
12. Stankovich, S.; *et al.* Graphene-Based Composite Materials. *Nature* **2006**, *442*, 282–286.
13. Obrzut, J.; Migler, K. B. Optical and Conductivity Properties from Liquid Phase Exfoliation of Natural Graphene. *Graphene and Emerging Materials for Post-CMOS Applications*; ECS: Pennington, NJ, 2009; Vol. 19, pp 69−73.
14. Rao, C. N. R.; Biswas, K.; Subrahmanyam, K. S.; Govindaraj, A. Graphene, The New Nanocarbon. *J. Mater. Chem.* **2009**, *19*, 2457–2469.
15. McAllister, M. J.; *et al.* Single Sheet Functionalized Graphene by Oxidation and Thermal Expansion of Graphite. *Chem. Mater.* **2007**, *19*, 4396–4404.
16. Schniepp, H. C.; Kudin, K. N.; Li, J.-L.; Prud'homme, R. K.; Car, R.; Saville, D. A.; Aksay, I. A. Bending Properties of Single Functionalized Graphene Sheets Probed by Atomic Force Microscopy. *ACS Nano* **2008**, *2*, 2577–2584.

17. Schniepp, H. C.; *et al.* Functionalized Single Graphene Sheets Derived from Splitting Graphite Oxide. *J. Phys. Chem. B* **2006**, *110*, 8535–8539.
18. Chen, G.; Weng, W.; Wu, D.; Wu, C. PMMA/Graphite Nanosheets Composite and Its Conducting Properties. *Eur. Polym. J.* **2003**, *39*, 2329–2335.
19. Miller, S. G.; Bauer, J. L.; Maryanski, M. J.; Heimann, P. J.; Barlow, J. P.; Gosau, J.-M.; Allred, R. E. Characterization of Epoxy Functionalized Graphite Nanoparticles and the Physical Properties of Epoxy Matrix Nanocomposites. *Compos. Sci. Technol.* **2010**, *70*, 1120–1125.
20. Fang, M.; Wang, K.; Lu, H.; Yang, Y.; Nutt, S. Single-Layer Graphene Nanosheets with Controlled Grafting of Polymer Chains. *J. Mater. Chem.* **2010**, *20*, 1982–1992.
21. Liang, J.; Huang, Y.; Zhang, L.; Wang, Y.; Ma, Y.; Guo, T.; Chen, Y. Molecular-Level Dispersion of Graphene into Poly(vinyl alcohol) and Effective Reinforcement of Their Nanocomposites. *Adv. Funct. Mater.* **2009**, *19*, 2297–2302.
22. Kim, H.; Macosko, C. W. Processing-Property Relationships of Polycarbonate/Graphene Composites. *Polymer* **2009**, *50*, 3797–3809.
23. Stauffer, D. *Introduction to Percolation Theory*; Taylor & Francis: London, 1985.
24. Kirkpatrick, S. Percolation and Conduction. *Rev. Mod. Phys.* **1973**, *45*, 574–588.
25. McLachlan, D. S.; *et al.* The Characteristics of Carbon Nanotube-Reinforced Poly(phenylene sulfide) Nanocomposites. *J. Polym. Sci., Part B* **2005**, *43*, 3273.
26. Tchoul, M. N.; *et al.* Composites of Single-Walled Carbon Nanotubes and Polystyrene: Preparation and Electrical Conductivity. *Chem. Mater.* **2008**, *20*, 3120–3126.
27. Barrau, S.; Demont, P.; Peigney, A.; Laurent, C.; Lacabanne, C. DC and AC Conductivity of Carbon Nanotubes-Polyepoxy Composites. *Macromolecules* **2003**, *36*, 5187–5194.
28. Kilbride, B. E.; *et al.* Experimental Observation of Scaling Laws for Alternating Current and Direct Current Conductivity in Polymer-Carbon Nanotube Composite Thin Films. *J. Appl. Phys.* **2002**, *92*, 4024–4030.
29. Reghu, M.; Yoon, C. O.; Yang, C. Y.; Moses, D.; Smith, P.; Heeger, A. J. Transport in Polyaniline Networks near the Percolation Threshold. *Phys. Rev. B* **1994**, *50*, 13931–13941.
30. Fraysse, J.; Planes, J. Interplay of Hopping and Percolation in Organic Conducting Blends. *Phys. Status Solidi B* **2000**, *218*, 273–277.
31. Arlen, M. J.; *et al.* Thermal-Electrical Character of *In-Situ* Synthesized Polyimide-Grafted Carbon Nanofiber Composites. *Macromolecules* **2008**, *41*, 8053–8062.
32. Dutta, P.; Biswas, S.; Ghosh, M.; De, S. K.; Chatterjee, S. The DC and AC Conductivity of Polyaniline-Polyvinyl Alcohol Blends. *Synth. Met.* **2001**, *122*, 455–461.
33. Linares, A.; *et al.* Broad-Band Electrical Conductivity of High Density Polyethylene Nanocomposites with Carbon Nanoadditives: Multiwall Carbon Nanotubes and Carbon Nanofibers. *Macromolecules* **2008**, *41*, 7090–7097.
34. Nogales, A.; *et al.* Low Percolation Threshold in Nanocomposites Based on Oxidized Single Wall Carbon Nanotubes and Poly(butylene terephthalate). *Macromolecules* **2004**, *37*, 7669–7672.
35. Dyre, J. C.; Schroder, T. B. Universality of AC Conduction in Disordered Solids. *Rev. Mod. Phys.* **2000**, *72*, 873–892.
36. Dyre, J. C. The Random Free Energy Barrier Model for AC Conduction in Disordered Solids. *J. Appl. Phys.* **1988**, *64*, 2456–2468.
37. Guinier, A.; Fournet, G. *Small-Angle Scattering of X-rays*; John Wiley and Sons: New York, 1955.
38. Higgins, J. S.; Benoit, H. C. *Polymers and Neutron Scattering*; Clarendon Press: Oxford, 1994.
39. Porod, G. In *Small-Angle X-ray Scattering*; Glatter, O., Kratky, O., Eds.; Academic Press: London, 1982.
40. Ho, D. L.; Briber, R. M.; Glinka, C. J. Characterization of Organically Modified Clays Using Scattering and Microscopy Techniques. *Chem. Mater.* **2001**, *13*, 1923–1931.
41. Yoonessi, M.; Toghiani, H.; Daulton, T. L.; Lin, J.-S.; Pittman Jr, C. U. Clay Delamination in Clay/Poly(dicyclopentadiene) Nanocomposites Quantified by Small Angle Neutron Scattering and High-Resolution Transmission Electron Microscopy. *Macromolecules* **2005**, *38*, 818–831.